Available online at www.sciencedirect.com

ScienceDirect

Procedia Structural Integrity 28 (2020) 525–537

Structural Integrity Procedia

www.elsevier.com/locate/procedia

1st Virtual European Conference on Fracture

Material Model Characterization of a Ti/SiC Metal Matrix Nanocomposite Coating Subjected to Hypervelocity Impact

Pouya Shojaei[a], Riccardo Scazzosi[b*], Mohamed Trabia[a], Brendan O'Toole[a], Marco Giglio[b], Xing Zhang[c], Yiliang Liao[c], Andrea Manes[b]

[a]*Department of Mechanical Engineering, University of Nevada, Las Vegas, 4505 S. Maryland, Pkwy, Las Vegas, NV, 89154, USA*
[b]*Politecnico di Milano, Department of Mechanical Engineering, via la Masa, 1, 20156, Milan, Italy*
[c] *Department of Mechanical Engineering, University of Nevada, Reno; 1664 N Virginia St, Reno, NV 89557, USA*

Abstract

Titanium alloys have been extensively used in the aerospace industry because of their outstanding properties, such as high strength-to-weight ratios, high corrosion resistances, and high melting points. However, it is hypothesized that the performance of titanium alloys can be further enhanced to be more resistant to hypervelocity impact by coating them. Earlier experimental investigations showed that coating a Ti-6Al-4V substrate by Ti/SiC Metal Matrix Nanocomposite (MMNC) improved hypervelocity impact resistance of the composite. The coating had 7% SiC by volume. These experiments were simulated using the Smoothed Particle Hydrodynamics (SPH) modeling approach. Johnson-Cook material models were used for the Ti-6Al-4V substrate and the Lexan projectile. Due to the lack of detailed mechanical characterization of the MMNC, a bilinear elastic plastic material model was used to model the coating. In this study, single-parameter sensitivity analyses were conducted to understand the sensitivity of the SPH model based on comparison with the experimental crater volume. The parameters of the bilinear elastic plastic material model were modulus of elasticity, Poisson's ratio, yield strength, tangent modulus, and the failure strain. These parameters were varied by ±5%, and ±10% of their respective base values for a Ti/SiC Metal Matrix Nanocomposite (MMNC) with 35% SiC by volume for which stress-strain curves under various strain rates were available. These values were applied to the full range of tested velocities. Exploiting the parameters from sensitivity analyses, the results show that the accuracy of SPH modeling of MMNC can be enhanced when experimental data is not available. The results also show that bilinear elastic plastic material model can be used for MMNC coating under elevated strain rates.

Keywords: Hypervelocity Impact; Ti/SiC Metal Matrix Nanocomposite; Coating; Smoothed Particle Hydrodynamics

* Corresponding author: Tel.: +39-02-2399-8630; fax: +39-02-2399-8263
E-mail address: riccardo.scazzosi@polimi.it

10.1016/j.prostr.2020.10.062

Nomenclature

a	First order volume correction factor to γ_0
A, B, C, n, m	Material constants in Johnson-Cook material model
C	Hugoniot intercept of the metal
E	Young's modulus
E_i	Absolute internal energy
ETAN	Tangent modulus
h	Crater depth
P	Pressure
PSFAIL	Failure strain
r	Crater radius
S1, S2, S3	Coefficient of slope of shock, and the particle velocity curve
SIGY	Yield strength
T^*	Homologous temperature
T_m	Melting temperature
T_r	Room temperature
γ_0	Grüneisen coefficient
ε^P	Effective plastic strain
$\dot{\varepsilon}^*$	Effective total strain-rate normalized by the quasi-static strain rate
ν	Poisson's ratio
ρ	Density
σ_y	Flow stress

1. Introduction

Titanium alloys are commonly used in aerospace applications due to their outstanding mechanical properties, such as high strength-to-weight ratios, desirable corrosion resistance, and superior strength at room and elevated temperatures [1-2]. Collisions of micrometeoroids and orbital debris traveling with velocities around 10 km/s are potential risks to the stability and integrity of the spacecrafts [3-6]. Ongoing attempts are being made to enhance the performance of structural components, including titanium alloys, subjected to hypervelocity impacts. The following is a brief survey of these efforts. Some researchers have studied the Whipple shields with different composite materials for protection against the hypervelocity impacts. For instance, Ren et al. [7] compared the hypervelocity impact-induced characteristics of Whipple shields with PTFE/Al, PTFE/Ti and Al2024 composites. The experimental results showed that the protective capability of PTFE/Al and PTFE/Ti reactive materials was better than that of Al2024, and the protective capability of PTFE/Al reactive material was better than that of PTFE/Ti. Zhang et al. [8] presented a meteoroid/debris shielding structure for spacecraft, using a bumper made of Ti-Al-nylon impedance-graded materials and an aluminum Whipple shield. They found that shielding capability of the Ti-Al-nylon was greater than that of an aluminum Whipple shield. Cherniaev et al. [9] evaluated the potential of coating aluminum substrates with ultrathin silicon carbide as substitutes for aluminum bumpers in orbital debris shielding. Hydrocode simulations were used to investigate the shielding capabilities of the proposed composite with two aluminum bumpers. The proposed laminated bumpers provided better hypervelocity projectile fragmentation. Gregori et al. [10] developed analytical and numerical models to simulate the perforation of pure alumina single tiles and multilayer Al2O3-Kevlar 29/epoxy composite targets by small-caliber projectiles. Cha et al. [11] proposed a Whipple shield design comprising of ultra-high-molecular-weight polyethylene (UHMWPE) to improve the space debris impact shielding efficiency over conventional Whipple shields. The ballistic performance of UHMWPE was better than Kevlar. However, ballistic performance of UHMWPE was degraded at temperatures usually encountered in space.

Nanocomposite particles have been increasingly used to enhance the performance of structural alloys in different applications [12-14]. For example, dispersion of reinforced Nano-ceramic particles into Ti-matrix in the form of Ti-based metal matrix nanocomposites (MMNCs) can improve the strength, high temperature stability, wear and fatigue resistance, combined with maintaining desirable ductility and toughness of the interior bulk material [15-17]. Some

researchers have focused on the effect of coating on the improvement of hypervelocity impact resistance. Xue et al. [18] designed SiC coated C/C (SiC-C/C) composites to evaluate the effects of hypervelocity impact on ablation behavior of coated carbon/carbon (C/C) composites. Mass ablation rates of SiC-C/C composites were lower than those of C/C composites under the same test condition. However, linear ablation rates of SiC-C/C composites were higher than those of C/C composites after the same impact tests. Li et al. [19] observed that the diameter of the penetration hole in carbon fiber reinforced SiC-matrix composites increased with increasing the impact velocity. In addition, low temperature induced smooth fracture, and decreased the diameters of damage zone, fragments and penetration hole. Kumar et al. [20] found Polybenzimidazole (PBI)-coated composites effective in increasing the energy absorption and reducing the mass loss and surface erosion under hypervelocity impact experiments. Nam et al. [21] proposed a silver-coated aramid/epoxy hypervelocity impact shielding system containing electromagnetic wave absorption capability and impact shielding system. The impact shielding performance was evaluated by hypervelocity impact experiments ranging between 2.7 and 3.2 km/s. The proposed system was promising for military satellite systems.

Among various surface modification techniques, selective laser melting (SLM) has a promising potential. During SLM processing of MMNCs, micro-scale powder of a metal is mixed with a Nano-scale particle and spread on a substrate plate. A high-energy laser beam is then applied to melt the powder layer. By repeating the powder deposition and laser melting processes, multilayer structure can be achieved. In a previous study, a Ti-6Al-4V substrate was coated with a 200-micron thickness Ti/SiC MMNC using SLM technique. The coating showed promising surface hardness, coefficient of friction, and wear rate [22-23]. Additional information about the specimen preparation can be found in [22].

Lagrangian Finite Element approaches have been used extensively in low-velocity impact simulations [24-25]. However, localized large deformations and material erosion associated with hypervelocity makes these approaches unsuitable. Smoothed Particle Hydrodynamics (SPH), which is a meshless approach, has shown high accuracy in modeling the hypervelocity impact events. In this approach, the bodies are discretized with particles with spatial distances. These particles interact through a kernel function with characteristic radius known as the "smoothing length. The quantity of any particle is obtained by summing the relevant properties of all the particles lying within the range of the kernel. In SPH formulation, the particles of the neighboring parts should have the same masses. Hence, careful evaluation should be used to ensure that the masses of particles on interacting parts are almost the same. The following is a brief overview of research in modeling the hypervelocity impacts using SPH approach. Livingstone et al. [26] developed a SPH numerical model to predict the fragmentation of metallic projectiles at impact velocities of 3.6 km/s and 4.5 km/s. O'Toole et al. [27] compared the Lagrangian-based SPH and the Eulerian-based CTH techniques in simulating impact experiments in the range of a few km/s. Both simulation techniques showed reasonable agreement of the physical measurements of impact cratering and bulge within ±8% error. Roy et al. [28] simulated hypervelocity impacts ranging from 5.1 to 5.4 km/s using SPH technique and Eulerian-based hydrocode. Both approaches were able to capture the physical measurements of impact cratering and the velocity profiles of the photonic Doppler velocimetry (PDV) experiments accurately. Wen et al. [29] utilized a 2D axisymmetric SPH model to estimate the geometric features of the wave front as a function of time and impact velocity in the hypervelocity impacts of thin flat targets. Scazzosi et al. [30] developed a numerical model combining Finite Element and SPH approaches to deal with crack formation and fracturing in the simulation of high-velocity impacts on ceramics.

In earlier study [31], a two-stage light gas gun was used for conducting the hypervelocity experiments. The Ti/SiC MMNC coating improved the hypervelocity impact resistance of the Ti-6Al-4V substrate ranging from 3.7 to 5.4 km/s. In this study, hypervelocity damage in the coated Ti-6Al-4V substrate is evaluated using an axisymmetric SPH model developed in LS-DYNA explicit solver. Ti-6Al-4V substrate and the Lexan projectile were modeled using Johnson-Cook material models. Bilinear elastic plastic material model with failure strain was used for modeling the MMNC coating. As experimental stress-strain data for the coated Ti/SiC MMNC were unavailable, the accuracy of SPH modeling of the MMNC, developed in [31], needed to be improved.

In this work, a series of single-parameter sensitivity analysis was performed to understand the sensitivity of crater volume measurement with respect to the MMNC input material model parameters. The MMNC coating material model variables were modulus of elasticity, Poisson's ratio, yield strength, tangent modulus, and the failure strain. These variables were varied with respect to their corresponding values for a Ti/SiC MMNC with 35% SiC by volume [32]. The analyses were performed based on the comparison with experimental crater volume at different range of velocities. The outline of the paper is as follows: the numerical model details are given in Section 2. Section 3 presents the results and discussion, and the conclusion is provided in Section 4.

2. Numerical Model

To evaluate hypervelocity damage in a Ti-6Al-4V substrate coated with Ti/SiC MMNC, a computational model was developed within LS-DYNA R 11.0 explicit code [33]. A 2D axisymmetric SPH computational model was developed for this study since it has already demonstrated high accuracy, along with computational cost benefits. The simulations were performed using MPP version with 8 processors.

The Ti-6Al-4V substrate used in the experiments had dimensions of 76.2mm x 68.58mm x 12.7mm, while a 200-micron thickness Ti/SiC MMNC coating was applied on a square region with an approximate area of 1600 mm^2. As observed in the earlier experimental studies [34], [28], the damage was localized, with no penetration of the plate. The most important part of the impact event happens in the first 10 microseconds of the impact. Additionally, the shock front does not reach the boundaries of the target plates during this time. Therefore, no boundary conditions were added to the model. An area with radius of 45 mm was used to model the experiment. The full thickness of the substrate was maintained in the model. Hence, the SPH models had the following dimensions: Ti-6Al-4V substrate was 45.0mm x 12.5mm, MMNC coating was 20.0mm x 0.2mm, and projectile was 2.75mm x 8.6mm, as shown in Figure 1. After comparing the crater size for models with different number of particles, the model with the closest results to experimental results at the highest hypervelocity testing was selected for the remainder of this research. Number of particles in each part is listed at Table 1. For initial conditions, equal initial velocities were assigned to each particle on the projectile particles. The lowest projectile particles were initially 0.4 mm away from the top MMNC coating particles. To dampen the numerical noise associated with the shock, an artificial bulk viscosity was applied using a linear viscosity coefficient of 1.0 and a quadratic viscosity coefficient of 1.5 [28], [35]. The SPH model is shown in Figure 1.

Table 1. Characteristics of SPH model

Part	Ti-6Al-4V Substrate	Projectile	MMNC Coating
Number of Particles	475 x 112	13 x 40	208 x 2

2.1. Equation of State (EOS)

The general thermodynamic relation accounting for the behavior of materials under shock conditions can be represented using the EOS, which incorporates pressure, temperature, internal energy, and density changes in front of the shock wave. Among the different forms of EOSs, the Grüneisen model was applied for describing the dynamic behavior of the Lexan projectile and the Ti-6Al-4V substrate. In the Grüneisen EOS model, the pressure formulation is expressed as [36]:

$$P = \frac{\rho_0 C^2 \mu [1+\left(1-\frac{\gamma_0}{2}\right)\mu - \frac{a}{2}\mu^2]}{[1-(S_1-1)\mu - S_2\frac{\mu^2}{\mu+1} - S_3\frac{\mu^3}{(\mu+1)^2}]^2} + (\gamma_0 + a\mu)E_i \quad (1)$$

where $\mu = \left(\frac{\rho}{\rho_0}\right) - 1$. EOS model parameters for the Lexan projectile and the Ti-6Al-4V substrate are summarized in Table 2.

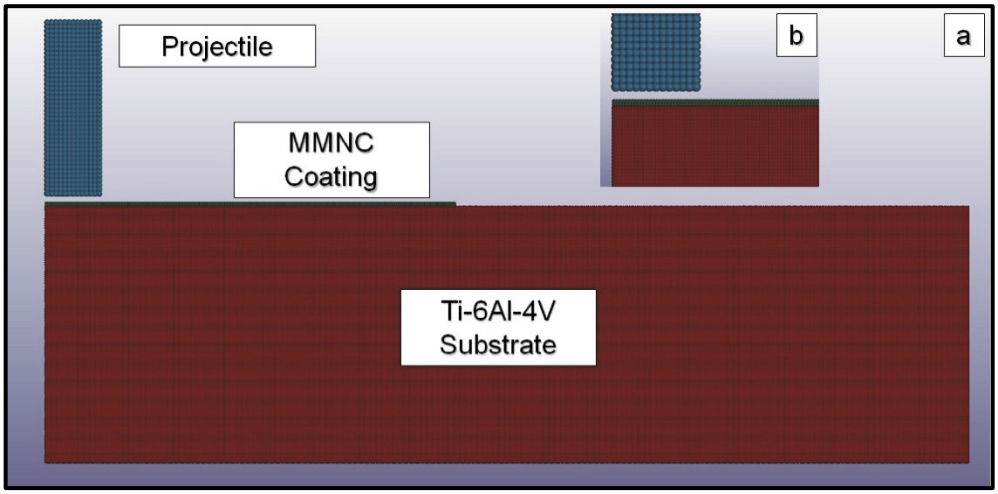

Figure 1. Axisymmetric model of the coated Ti-6Al-4V substrate (45.0mm x 12.5mm), MMNC coating (20.0mm x 0.2mm), and projectile (2.75mm x 8.6mm) (a) Overall model and (b) Zoomed view

Table 2. Gruneisen EOS parameters for Lexan, and Ti-6Al-4V alloy

Material	$\rho\ (\frac{kg}{m^3})$	$C\ (\frac{m}{s})$	S_1	γ_0
Lexan [29]	1190	1933	1.42	0.61
Ti-6Al-4V [37]	4428	5130	1.028	1.23

2.2. Material Models

2.2.1. Johnson-Cook Material Model

The Johnson-Cook material model is typically used for problems where the strain rates vary over a large range. This material model accounts for adiabatic temperature increases caused by energy release during impact, which is observed in the form of material softening. The flow stress of this material model is expressed as [38]:

$$\sigma_y = (A + B(\varepsilon^P)^n)(1 + Cln(\dot{\varepsilon}^*))(1 - (T^*)^m) \tag{2}$$

where $T^*$is defined as:

$$T^* = \frac{T - T_r}{T_m - T_r} \tag{3}$$

The Johnson-Cook material model parameters for the Lexan and Ti-6Al-4V alloy are given in Table 3.

Table 3. Johnson-Cook material model parameters for Lexan, and Ti-6Al-4V alloy

Property	$\rho(\frac{kg}{m^3})$	$E(Pa)$	ν	$A(Pa)$	$B(Pa)$	C	n	m
Lexan Projectile [39]	1190	2.54E9	0.34	7.54E7	6.89E7	0	1.00399	1.85
Ti-6Al-4V Substrate [37]	4428	109.8E9	0.311	1.098E9	1.092E9	0.014	0.93	1.1

2.2.2. Bilinear Elastic Plastic Material Model for MMNC Coating

Bilinear elastic plastic material model with failure strain was used for modeling the coating, which has a mixture of 5% SiC and 95% Ti by weight. This mixture is equivalent to 6.88% SiC and 93.12% Ti by volume. The density of the coating was calculated to be 4356 kg/m^3. Any accurate simulation study depends on the availability of material models. Since the actual coating material was not yet precisely calibrated, it was important to develop a model based on the closest available material where its characteristics are known: MMNC with 35% SiC and 65% Ti by volume, [32]. Based on the shape of the stress-strain curves of this composite under different strain rates, it was proposed to use a bilinear elastic plastic model with a failure strain for capturing the failure response of the coating. The baseline model parameters were obtained by applying linear regression fitting to the stress-strain curve at $\dot{\varepsilon} = 500\ s^{-1}$. These material model parameters are summarized in Table 4.

Table 4. Bilinear elastic plastic material model parameters for 35% SiC and 65% Ti MMNC coating

Property	$\rho(\frac{kg}{m^3})$	E(GPa)	ν	SIGY (MPa)	ETAN (GPa)	PSFAIL
MMNC Coating [32]	4356	266	0.31	1256	138.9	0.0059

2.3. Sensitivity Analysis Methodology

In this study, single-parameter sensitivity analysis was conducted on the bilinear elastic plastic material model parameters: modulus of elasticity, Poisson's ratio, yield strength, tangent modulus, and failure strain. The results of the sensitivity analysis were compared based on the closeness of the SPH crater volume to the crater volume in the experimental data. Crater diameter and depth were combined to calculate the crater volume, V. The crater volume was estimated using Eq. (4).

$$V = \frac{\pi}{6} h(3r^2 + h^2) \tag{4}$$

These input variables were varied by ±5%, and ±10% of the respective base values of Table 4. In total, 25 parameter combinations were simulated with the impact velocity of 4.448 km/s. Figure 2 shows the variables used to calculate the crater volume: the radius and depth, *r* and *h* respectively. A typical transition region was seen at the surface level of the coating, around the crater, which was distinguished by separation of particles. The radius was measured from the particles at the transitional region, denoted by *r* in Figure 2. The depth of the crater was measured as the vertical distance from the particles explained earlier to the uppermost particles at the center of symmetry, denoted by h in Figure 2.

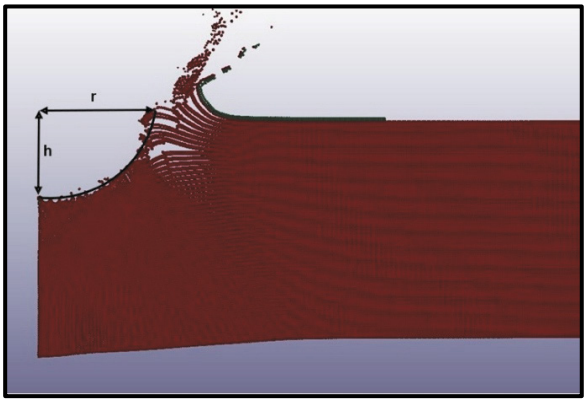

Figure 2. Analysis of numerical crater by measuring the radius (r) and height of the crater (h)

3. Discussion

The initial model developed in the [31] showed a reasonable agreement with the corresponding experiment. For example, for an impact velocity of 4.448 km/s, this model predicted a crater diameter of 17 mm and a crater depth of 4.3 mm with the error in the crater volume equal to +7.4%. Although this error was fairly low, a sensitivity analysis was designed to evaluate the effect of each parameter of the MMNC bilinear elastic plastic material model on improving the accuracy of the simulation. All these parameters were varied by -10%, -5%, 5%, and 10% respectively. The sensitivity analysis evaluates the effect of varying the elastic modulus, Poisson's ratio, yield stress, tangent modulus, and failure strain on the error of crater diameter and depth, as well as the crater volume.

The results of the sensitivity analysis are reported in Figures 3 through 7, respectively. Both the diameter and depth increase with the value of the elastic modulus. The results show the lowest errors of both the crater diameter and depth, occurring at -10% variation for all parameters except for the failure strain, where the behavior reversed.

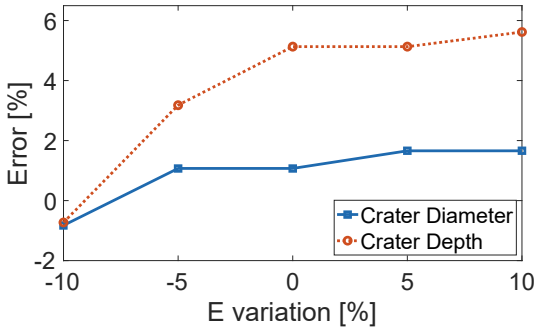

Figure 3. Elastic modulus sensitivity analysis (V = 4.448 km/s)

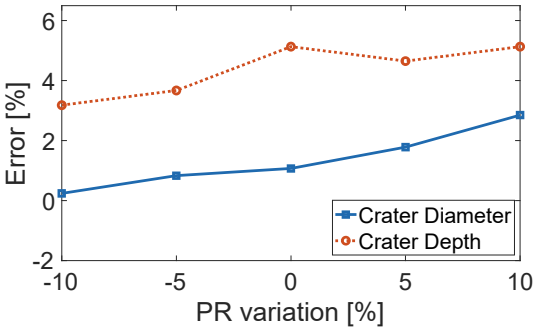

Figure 4. Poisson's ratio sensitivity analysis (V = 4.448 km/s)

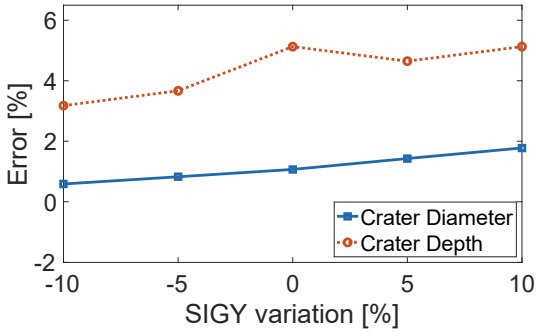

Figure 5. Yield stress sensitivity analysis (V = 4.448 km/s)

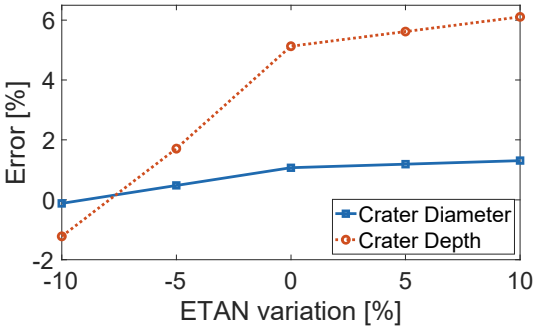

Figure 6. Tangent modulus sensitivity analysis (V = 4.448 km/s)

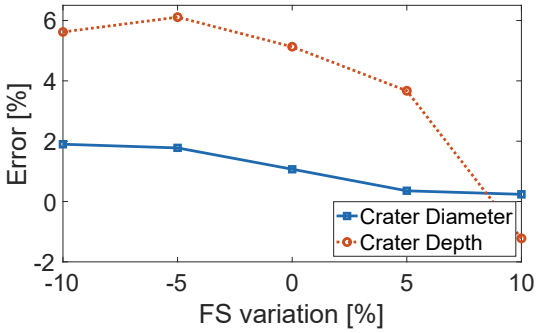

Figure 7. Failure strain sensitivity analysis (V = 4.448 km/s)

The error percentages of the crater volume for the studied cases at V=4.448 km/s are shown in Table 5. The results confirm those of Figures 3 through 7. These results were, to some extent, expected as the parameters of Table 4 were for a SiC volume fraction of 35%, while the SiC volume fraction of the MMNC coating was only 6.88%. Hence, lower elastic modulus and yield stress and higher failure strain were justified. Additionally, the strain rates in this experiment (10^5 to 10^6 s^{-1}) were of a higher order than what was reported in [32] (500 s^{-1}). This led to having two competing effects on the tangent modulus and failure strain: change of the SiC volume percentage and strain rate.

Table 5. Error in the prediction of the crater volume (V = 4.448 km/s)

Input parameter variation	Crater Volume Error for Each Input Parameter				
	E	PR	SIGY	ETAN	FS
-10%	-2.4%	4.1%	4.8%	-1.6%	10.3%
-5%	5.7%	5.8%	5.8%	2.9%	10.6%
0%	8.0%	8.0%	8.0%	8.0%	8.0%
5%	9.2%	8.9%	8.2%	8.9%	4.9%
10%	9.8%	11.6%	9.5%	9.7%	-1.0%

The best parameters (elastic modulus, Poisson's ratio, yield stress, tangent modulus with -10% variation, and failure strain with +10% variation) were defined as Sets 1-5, Table 6. In addition, Set 6 was defined to include the variations in Sets 1-5 together. The results of material models of Table 6 were compared with the corresponding experiments at different velocities, shown in Figure 8. For each set of input parameters, the error increases with increasing the impact velocity. However, the variation of the errors is fairly low. Sets 2 and 3 slightly overestimate the crater volume and the overestimation barely increases with the impact velocity. Set 6 predicts the crater volume with the error of 1.0 to 2.3% over the range of velocities. Sets 1, 4 and 5 slightly underestimate the crater volume and the underestimation increases by increasing the impact velocity. Among Sets 4, 5, and 6, which provided the most accurate results, the error produced by Set 5 is the most stable one in the range of tested velocities. The average errors on prediction of the crater volume at different impact velocities has been reduced from +7.4% using the initial model parameters to -1.1% using the Set 5 parameters.

The impacted coated target plate at V=4.448 km/s is shown in Figure 9. At this velocity, the numerical simulations showed a relatively small peak along the axis of symmetry which agreed with the hypervelocity tested specimen. In Figure 10, the overlaid crater profile of Set 5 with experimental cross section at V=4.448 km/s is compared with the results of the initial model to assess the improvements.

Table 6. Best sets of input parameters

Set	E		PR		SIGY		ETAN		FS	
	Variation (%)	Value (GPa)	Variation (%)	Value	Variation (%)	Value (GPa)	Variation (%)	Value (GPa)	Variation (%)	Value
1	-10%	239.4	0%	0.31	0%	1.256	0%	138.9	0%	0.0059
2	0%	266	-10%	0.28	0%	1.256	0%	138.9	0%	0.0059
3	0%	266	0%	0.31	-10%	1.130	0%	138.9	0%	0.0059
4	0%	266	0%	0.31	0%	1.256	-10%	125	0%	0.0059
5	0%	266	0%	0.31	0%	1.256	0%	138.9	+10%	0.0065
6	-10%	239.4	-10%	0.28	-10%	1.130	-10%	125	+10%	0.0065

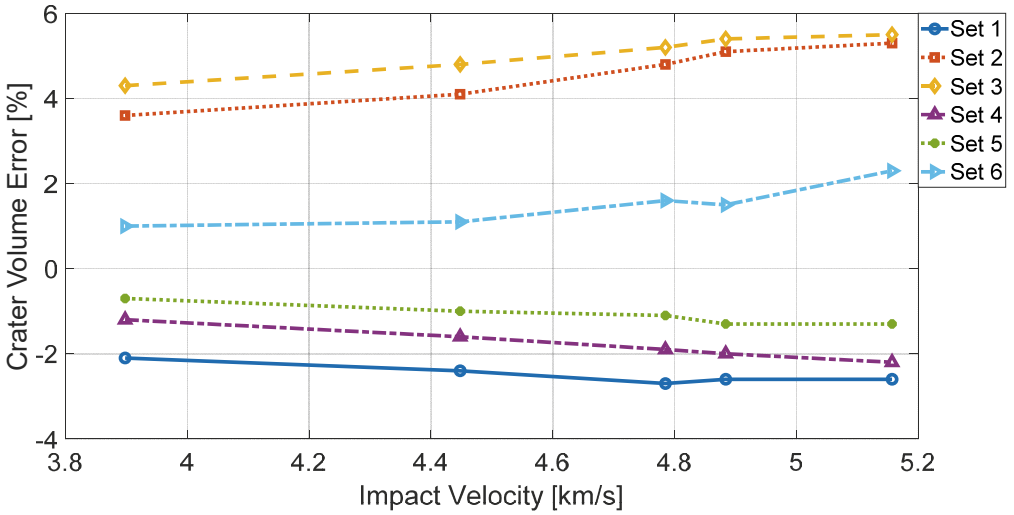

Figure 8. Crater volume error for different impact velocities considering the sets of input parameters of Table 6

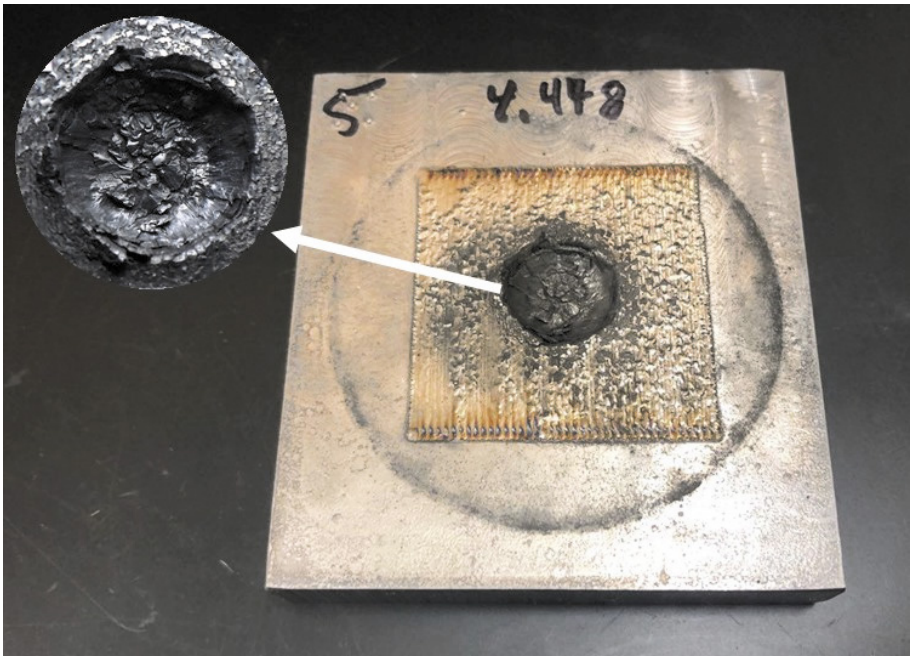

Figure 9. Coated target plate impacted at V=4.448 km/s

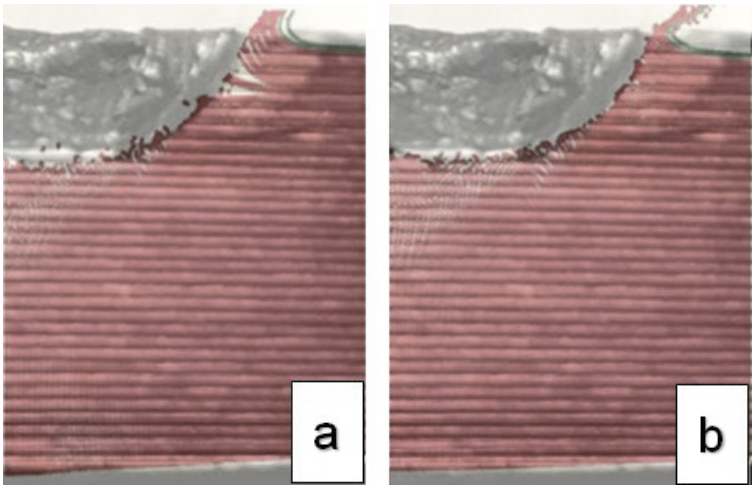

Figure 10. Overlaid numerical and experimental cross section figures of (a) Initial baseline SPH model (b) Optimized SPH model (Set 5) at V=4.448 km/s

4. Conclusion

The Ti/SiC Metal Matrix Nanocomposite coating with 6.88% volume SiC was experimentally proven to enhance the hypervelocity impact resistance of a Ti-6Al-4V substrate. As the detailed mechanical characterization of the MMNC coating was unavailable in the literature, the properties of a Ti/SiC MMNC with 35% SiC by volume was already used as the baseline in SPH simulation. The baseline parameters showed good agreement with the experimental crater volume measurements, however a specific investigation on the actual coating was considered of interest in order to improve the accuracy of the numerical prediction. In this study, it was proposed to conduct a single-parameter sensitivity analyses on the bilinear elastic plastic material model parameters to improve the accuracy of the SPH model in predicting the crater measurements with respect to the experimental results. The parameters of the bilinear elastic plastic material model were modulus of elasticity, Poisson's ratio, yield strength, tangent modulus, and the failure strain. These parameters were varied from -10% to +10% of their respective baseline values. The material model parameters were then studied in the range of hypervelocity impact experiments (3.9 to 5.2 km/s). The single-parameter sensitivity analyses showed that reducing the modulus of elasticity, Poisson's ratio, yield strength, and tangent modulus by 10% while increasing the failure strain by 10% improved the accuracy of the models. All the above variations were also applied at the same time as another case (called Set 6 herein). Among the studied cases, reducing the tangent modulus by 10% (called Set 4 herein), increasing the failure strain by 10% (called Set 5 herein) and Set 6 provided the best results. Among these cases, Set 5 showed the most stable error percentage over the range of impact velocities (-1.3% to -0.7%). The results showed that the accuracy of SPH modeling of MMNC can be enhanced in the absence of characterization experiments. It was also seen that the optimized SPH models' crater volume were closer to the experimental crater measurements. As an example, the average errors on prediction of the crater volume at different impact velocities was reduced from +7.4% using the baseline model parameters to -1.1% using the Set 5 parameters. It was shown that the bilinear elastic plastic material model can be used for modeling the MMNC coating under elevated strain rates.

Acknowledgements

This work was partially supported by a NV NASA EPSCoR Research Infrastructure Development Seed Grant under award # NNX15AK48A and NASA Marshall Space Flight Center (MSFC) Office of the Chief Technologist SCP award.

The authors also acknowledge the Texas Advanced Computing Center (TACC) at The University of Texas at Austin for providing HPC resources that have contributed to the research results reported within this paper. URL:

http://www.tacc.utexas.edu.

References

[1]Sun F, Huang L, Zhang R, Wang S, Jiang S, Sun Y, et al. In-situ synthesis and superhigh modulus of network structured TiC/Ti composites based on diamond-Ti system. J Alloys Compd 2020;834:1–11. https://doi.org/10.1016/j.jallcom.2020.155248.

[2]Ryan S, Christiansen EL. Hypervelocity impact testing of advanced materials and structures for micrometeoroid and orbital debris shielding. Acta Astronaut 2013;83:216–31. https://doi.org/10.1016/j.actaastro.2012.09.012.

[3]Schonberg WP, Walker EJ. Use of composite materials in multi-wall structures to prevent perforation by hypervelocity particle impact. Compos Struct 1991;19:15–40. https://doi.org/https://doi.org/10.1016/0263-8223(91)90073-8.

[4]Christiansen EL, Nagy K, Lear DM, Prior TG. Space station MMOD shielding. Acta Astronaut 2009;65:921–9. https://doi.org/10.1016/j.actaastro.2008.01.046.

[5]Nishida M, Hongo A, Hiraiwa Y, Higashide M. Effects of gamma ray irradiation on penetration hole in and fragment size from carbon fiber reinforced composite plates in hypervelocity impacts. Compos Part B Eng 2019;169:229–38. https://doi.org/10.1016/j.compositesb.2019.04.007.

[6]Huang X, Yin C, Ru H, Zhao S, Deng Y, Guo Y, et al. Hypervelocity impact damage behavior of B4C/Al composite for MMOD shielding application. Mater Des 2020;186:108323. https://doi.org/10.1016/j.matdes.2019.108323.

[7]Ren S, Zhang Q, Wu Q, Xue Y, Zheng K, Lu Y, et al. Influence of impact-induced reaction characteristics of reactive composites on hypervelocity impact resistance. Mater Des 2020;192:108722. https://doi.org/10.1016/j.matdes.2020.108722.

[8]Zhang PL, Xu KB, Li M, Gong ZZ, Song GM, Wu Q, et al. Study of the shielding performance of a Whipple shield enhanced by Ti-Al-nylon impedance-graded materials. Int J Impact Eng 2019;124:23–30. https://doi.org/10.1016/j.ijimpeng.2018.08.005.

[9]Cherniaev A, Telichev I. Sacrificial bumpers with high-impedance ceramic coating for orbital debris shielding: A preliminary experimental and numerical study. Int J Impact Eng 2018;119:45–56. https://doi.org/10.1016/j.ijimpeng.2018.05.004.

[10] Gregori D, Scazzosi R, Nunes SG, Amico SC, Giglio M, Manes A. Analytical and numerical modelling of high-velocity impact on multilayer alumina/aramid fiber composite ballistic shields: Improvement in modelling approaches. Compos Part B Eng 2020;187:107830. https://doi.org/10.1016/j.compositesb.2020.107830.

[11] Cha JH, Kim YH, Sathish Kumar SK, Choi C, Kim CG. Ultra-high-molecular-weight polyethylene as a hypervelocity impact shielding material for space structures. Acta Astronaut 2020;168:182–90. https://doi.org/10.1016/j.actaastro.2019.12.008.

[12] Faria B, Guarda C, Silvestre N, Lopes JNC. CNT-reinforced iron and titanium nanocomposites: Strength and deformation mechanisms. Compos Part B Eng 2020;187. https://doi.org/10.1016/j.compositesb.2020.107836.

[13] Najafi F, Wang G, Mukherjee S, Cui T, Filleter T, Singh CV. Toughening of graphene-based polymer nanocomposites via tuning chemical functionalization. Compos Sci Technol 2020;194:108140. https://doi.org/10.1016/j.compscitech.2020.108140.

[14] Dolati S, Azarniya A, Azarniya A, Eslami-shahed H, Hosseini HRM, Simchi A. Toughening mechanisms of SiC-bonded CNT bulk nanocomposites prepared by spark plasma sintering. Int J Refract Met Hard Mater 2018;71:61–9. https://doi.org/10.1016/j.ijrmhm.2017.10.024.

[15] Hu Z, Chen F, Xu J, Ma Z, Guo H, Chen C, et al. Fabricating graphene-titanium composites by laser sintering PVA bonding graphene titanium coating: Microstructure and mechanical properties. Compos Part B Eng 2018;134:133–40. https://doi.org/10.1016/j.compositesb.2017.09.069.

[16] Zhang F, Liu T. Nanodiamonds reinforced titanium matrix nanocomposites with network architecture. Compos Part B Eng 2019;165:143–54. https://doi.org/10.1016/j.compositesb.2018.11.110.

[17] Gu D, Zhang H, Dai D, Xia M, Hong C, Poprawe R. Laser additive manufacturing of nano-TiC reinforced Ni-based nanocomposites with tailored microstructure and performance. Compos Part B Eng 2019;163:585–97. https://doi.org/10.1016/j.compositesb.2018.12.146.

[18] Xue LZ, Li KZ, Jia Y, Zhang SY, Ren JJ, You ZY. Effects of hypervelocity impact on ablation behavior of SiC coated C/C composites. Mater Des 2016;108:151–6. https://doi.org/10.1016/j.matdes.2016.06.106.
[19] Li T, Mo J, Yu X, Suo T, Li Y. Mechanical behavior of C/SiC composites under hypervelocity impact at different temperatures: Micro-structures, damage and mechanisms. Compos Part A Appl Sci Manuf 2016;88:19–26. https://doi.org/10.1016/j.compositesa.2016.05.015.
[20] Sathish Kumar SK, Jurado-Manriquez EA, Kim YH, Choi C, Baluch AH, Kim CG. Polybenzimidazole (PBI) film coating for improved hypervelocity impact energy absorption for space applications. Compos Struct 2018;188:72–7. https://doi.org/10.1016/j.compstruct.2017.12.052.
[21] Nam YW, Sathish Kumar SK, Ankem VA, Kim CG. Multi-functional aramid/epoxy composite for stealth space hypervelocity impact shielding system. Compos Struct 2018;193:113–20. https://doi.org/10.1016/j.compstruct.2018.03.046.
[22] Zhang X, Mao B, Histed R, Trabia M, O'Toole B, Jennings R, et al. Selective laser melting of Ti/SiC nanocomposite coating towards enhanced surface performance of Ti64. MS T 2019 - Mater. Sci. Technol. 2019, 2019. https://doi.org/10.7449/2019/MST_2019_356_363.
[23] Li N, Xiong Y, Xiong H, Shi G, Blackburn J, Liu W, et al. Microstructure, formation mechanism and property characterization of Ti + SiC laser cladded coatings on Ti6Al4V alloy. Mater Charact 2019;148:43–51. https://doi.org/10.1016/j.matchar.2018.11.032.
[24] Somasundaram DS, Shojaeishahmirzadi P, Trabia MB, O'Toole BJ. Shock propagation through a bolted joint structure under impact loading. Proc. 26th Int. Congr. Sound Vib. ICSV 2019, 2019.
[25] Shojaei P, Trabia M, O'Toole B. Effect of Bolted Joints on Shock Propagation across Structures under Medium Impact Loading. Proc. ASME 2019 Int. Mech. Eng. Congr. Expo., Salt Lake City: ASME; 2019.
[26] Livingstone IHG, Verolme K, Hayhurst CJ. Predicting the fragmentation onset velocity for different metallic projectiles using numerical simulations. Int J Impact Eng 2001;26:453–64. https://doi.org/10.1016/S0734-743X(01)00096-3.
[27] O'Toole B, Trabia M, Hixson R, Roy SK, Pena M, Becker S, et al. Modeling plastic deformation of steel plates in hypervelocity impact experiments. Procedia Eng 2015;103:458–65. https://doi.org/10.1016/j.proeng.2015.04.060.
[28] Roy SK, Trabia M, O'Toole B, Hixson R, Becker S, Pena M, et al. Study of Hypervelocity Projectile Impact on Thick Metal Plates. Shock Vib 2016;2016. https://doi.org/10.1155/2016/4313480.
[29] Wen K, Chen XW, Di DN. Modeling on the shock wave in spheres hypervelocity impact on flat plates. Def Technol 2019:0–9. https://doi.org/10.1016/j.dt.2019.01.006.
[30] Scazzosi R, Giglio M, Manes A. FE Coupled to SPH Numerical Model for the Simulation of High- Velocity Impact on Ceramic Based Ballistic Shields. Ceram Int 2020. https://doi.org/10.1016/j.ceramint.2020.06.151.
[31] Shojaei P, Trabia M, O'Toole B, Jennings R, Zhang X, Liao Y. Enhancing hypervelocity impact resistance of titanium substrate using Ti/SiC Metal Matrix Nanocomposite coating. Compos Part B Eng 2020. https://doi.org/https://doi.org/10.1016/j.compositesb.2020.108068.
[32] Gálvez F, González C, Poza P, LLorca J. The effect of strain rate on the tensile deformation of Ti-6Al-4V/SiC composites. Scr Mater 2001;44:2667–71. https://doi.org/10.1016/S1359-6462(01)00947-2.
[33] (LSTC) LSTC. LS-DYNA KEYWORD USER ' S MANUAL. vol. I. n.d.
[34] Matthes M, O'Toole B, Trabia M, Roy S, Jennings R, Bodenchak E, et al. Comparison of failure mechanisms due to shock propagation in forged, layered, and additive manufactured titanium alloy. Conf Proc Soc Exp Mech Ser 2017;1B:131–8. https://doi.org/10.1007/978-3-319-41132-3_18.
[35] Panciroli R. Hydroelastic Impacts of Deformable Wedges. In: Abrate S, Castanié B, Rajapakse YDS, editors. Dyn. Fail. Compos. Sandw. Struct., Dordrecht: Springer Netherlands; 2013, p. 1–45. https://doi.org/10.1007/978-94-007-5329-7_1.
[36] Hallquist JO. LS-DYNA3D theoretical manual. Livermore software technology corporation Livermore, Calif.; 1994.
[37] Wang X, Shi J. Validation of Johnson-Cook plasticity and damage model using impact experiment. Int J Impact Eng 2013;60:67–75. https://doi.org/10.1016/j.ijimpeng.2013.04.010.
[38] Autodyn A. Theory manual revision 4.3. Century Dyn Inc, Concord, CA 2005.

[39] Littlewood DJ. Simulation of Dynamic Fracture Using Peridynamics, Finite Element Modeling, and Contact 2010:209–17. https://doi.org/10.1115/IMECE2010-40621.